Chapter V

The Optical and Electrical Transport Studies of CoS and $Co_{1-x}Zn_xS$ Thin Films

5.1. Introduction

In recent years, thin chalcogenide films of II-VI, IV-VI, II-IV-VI, III-V and I-III-V compounds are emerged as the potential candidates of high performance and low production cost [1-13]. The electronic and optoelectronic properties of the binary and ternary semiconductor materials of group II-VI and IV-VI have been extensively studied due to their important non-linear luminescent properties and quantum size effect [1, 2, 11-15]. These materials are of importance owing to their close matching band gaps with the maximum span of the solar spectrum. Polycrystalline electrodes with a large area are economically desirable and have proved to be competent in solar cell applications. ZnS is a direct band gap material (E_g = 3.2 eV) and can be alloyed easily with CoS (E_g = 1.15 eV) to cope with the maximum span of the solar spectrum via band gap engineering, alteration in the composition, structure, morphology and allied surface, spectroscopic optical and transport properties [14-16]. A ternary system such as $Co_{1-x}Zn_XS$, composed of CoS and ZnS, therefore can be engineered for better application purposes by suitably choosing the composition parameter, x. The characterization of these thin film materials is the prime and key step in the fabrication and development of the devices. The properties of these thin film materials can be studied by using various characterization tools and techniques as mentioned earlier (Chapter-II). This chapter is fully devoted to the optical, electrical and transport studies on the CoS and $Co_{1-x}Zn_xS$ thin films. The

study of optical properties of the thin films has vital role because the optical properties determine the efficiency of the devices (particularly thin film based solar cells). Moreover, these are closely related to the composition of the films and therefore microstructural changes which are brought about by the method of synthesis involving several delicate parameters and some intentional additives. Measurement of the optical properties thus allow us to obtain critical assessment vis-à-vis electronic band structure, optical transitions and relaxation mechanism [4, 11-17].

For the development and assessment of the device quality films, it is also necessary to investigate the electrical transport characteristics. Knowledge of the electrical properties is must to know for understanding and correlating the factors affecting the device performance. Lifetime and mobility of the charge carriers have been identified as the main electrical parameters controlling the material performance. Impurities, grain boundaries and interfaces influence the electrical properties, which can be understood by analyzing the temperature dependent behaviour of an electrical conductivity. Electrical transport properties are sensitive to the stoichiometric deviations and hence it is pertinent to study the essential features of the as-grown CoS and $Co_{1-x}Zn_xS$ thin films via the optical and electrical characterization techniques [1, 3, 5, 9, 11, 12, 18-21]. In the present investigations, electrical characterization was done by the electrical conductivity and thermoelectric power measurement techniques.

5.2. Experimental Details

5.2.1. Deposition of the samples

The CoS and $Co_{1-x}Zn_xS$ ($0 \leq x \leq 0.4$) thin films were deposited onto the non-conducting glass substrates as described earlier (chapter III, section 3.2.2) [14-16]. It is based on slow release of Co^{2+}, Zn^{2+} ions from the complexed state and decomposition of thiourea in an aqueous ammonical solution (pH = 9.0 ± 0.1). Properly cleaned substrates were mounted on a substrate holder and rotated in reaction mixture at a speed of 65 ± 2 rpm. The temperature of the bath was allowed to increase slowly to 80°C. The detailed procedure is given in chapter III (Section 3.2.2).

5.2.2. UV-Vis measurements

The measurement on the absorption spectra of the thin film samples under investigation were carried out at room temperature. The absorbance was measured as a function of the wavelength without considering losses due to reflection and scattering. A BIO-AGE (2800 PC) UV-Vis spectrophotometer was used for this purpose. A substrate transmission correction was applied by placing an identical uncoated glass substrate as a reference. The transmission spectra were recorded in the 200 nm -1600 nm wavelength range in a steps of 2 nm. The spectra were used to calculate the absorption coefficient, energy band gap and the type of the optical transitions involved and also to calculate other related parameters.

5.2.3. Electrical conductivity measurements

The electrical measurements involve measurement of temperature dependence of dark conductivity. Dark conductivities for all the films were measured as a function of the temperature in the 300 K- 550 K temperature range. The films were prepared on the

glass substrates and electrical contacts were made using silver paint. Sample was slowly heated to 550 K at the rate of 2.5 K/min and the current flowing through the sample was measured at different temperatures during cooling.

5.2.4. Thermoelectric power measurements

The thermoelectric power measurements were carried out on these samples in the 300 K - 500 K temperature range. To sense the working temperature, a calibrated chromel-alumel thermocouple (24-gauge size) was used. The thermo-voltage was measured using a Hewlett-Packard, 6 ½-digit multimeter.

5.2.5. Photosensitivity measurements

At room temperature, the d.c. electrical conductivities under constant illumination ($5mW/cm^2$) were measured by a two-probe conductivity measuring unit. For this purpose, filters of different wavelengths were introduced in the pathway of the light incident on the sample. The resulting photocurrents at a fixed temperature were measured for various wavelengths. The conductivities of these samples in dark and in light were then calculated. From the observed conductivities, sensitivities of the materials were then determined. The photosensitivities were then calculated by taking the ratio of the photoconductivity to the dark conductivity.

5.3. Results and Discussion

5.3.1. Optical studies

A photon incident on any material may either be reflected, transmitted or absorbed. The phenomena of radiation absorption in a material is all together considered to be due to:

1) inner shell electrons, 2) valence band electrons, 3) free carriers including electrons and 4) electrons bound to the localized impurity centers or defects of some type. In the study of fundamental properties of the semiconductors, absorption by the second type of electrons is of great importance. In an ideal semiconductor at absolute zero temperature, the valence band would be completely full of electrons so that electron could not be excited to higher energy state. Absorption of quanta of sufficient energy tends to transfer of electrons from valence band to the conduction band. The optical absorption spectrum of the semiconductors generally exhibits a sharp rise at a certain value of the incident photon energy which can be attributed to the excitation of electrons from the valence band to conduction band (may also involve acceptor or donor impurity levels, traps, excitons, etc.). Light incident on the material is therefore absorbed if it can cause an electronic transition. In semiconductors, this process can occur by means of several mechanisms, including the following [1, 3, 4, 17, 22];

a) Direct interband (band-to-band) transitions
b) Indirect interband transitions
c) Impurity-to-band and impurity-impurity transitions
d) Excitonic transitions
e) Interband transitions
f) Phonon transitions.

Semiconductors absorb light with energy equal to or greater than their band gap. Thus, optical measurements constitute an important means of determining the band structures of the semiconductors. Measurement of the optical transmission in the binary and

ternary cobalt sulfide thin films in the wavelength range from 200 nm- 1600 nm at room temperature was therefore carried out. The absorption coefficient for each of the wavelengths was then calculated. The optical absorbances of the six representative films are plotted vs wavelength and are shown in fig. 5.1.

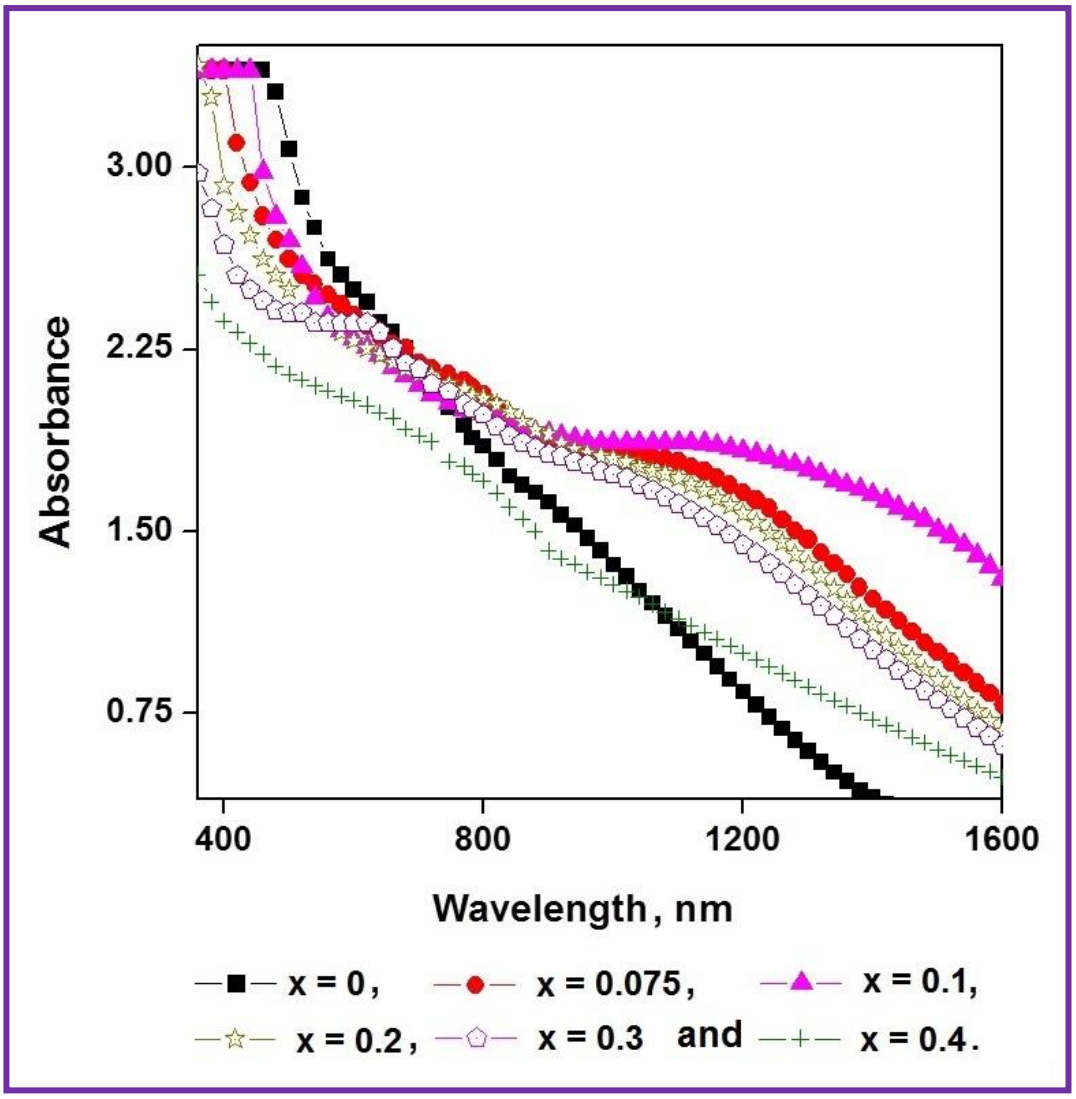

Figure 5.1. Variation of the absorbance vs wavelength (λ) for six representative Co-Zn-S thin film structures.

The spectra were used to evaluate the absorption coefficient (α), nature of the transition involved and optical band gap (Eg). The study showed the presence of an absorption edge of the exponential nature, which is a characteristic of II-VI compounds. It is due to homogeneity of the films and normal band structure. The spectra showed two regions; one for higher wavelengths with practically zero absorption and other for lower wavelengths in which absorption increases steeply [1, 3-10]. The wavelength dependence of an absorption coefficient (α) for CoS and $Co_{1-x}Zn_xS$ thin films is shown in fig. 5.2. From fig. 5.2, it appears that the optical absorption coefficient (α) is of the order of $\approx 10^4$ cm^{-1}. The composition dependence of α is represented in fig. 5.3. A systematic increase in α upto x = 0.3 is observed, which may be attributed to the creation of more localized states within the band tails of the valence and conduction bands due to the existence of defects and disorders. The lower wavelength shift in the absorption edge with the addition of Zn content can be explained with the sp-d exchange interaction between the band electrons in CoS and localized d electrons of Zn^{2+} [16, 23, 24]. In the present system, zinc plays a two-fold role. First, it occupies partially vacant Co sites and manipulates the defect states and second it forms a semiconducting alloy whose composition controls the band structure and lattice spacings. The absorption edge was then determined for all the compositions by extrapolating the steep portion of α vs λ plots on the wavelength axis. As the composition parameter (x) is increased, absorption shows an increasing trend with the wavelength and the fundamental edge is shifted towards smaller wavelengths. At higher wavelengths, absorption coefficient decreased.

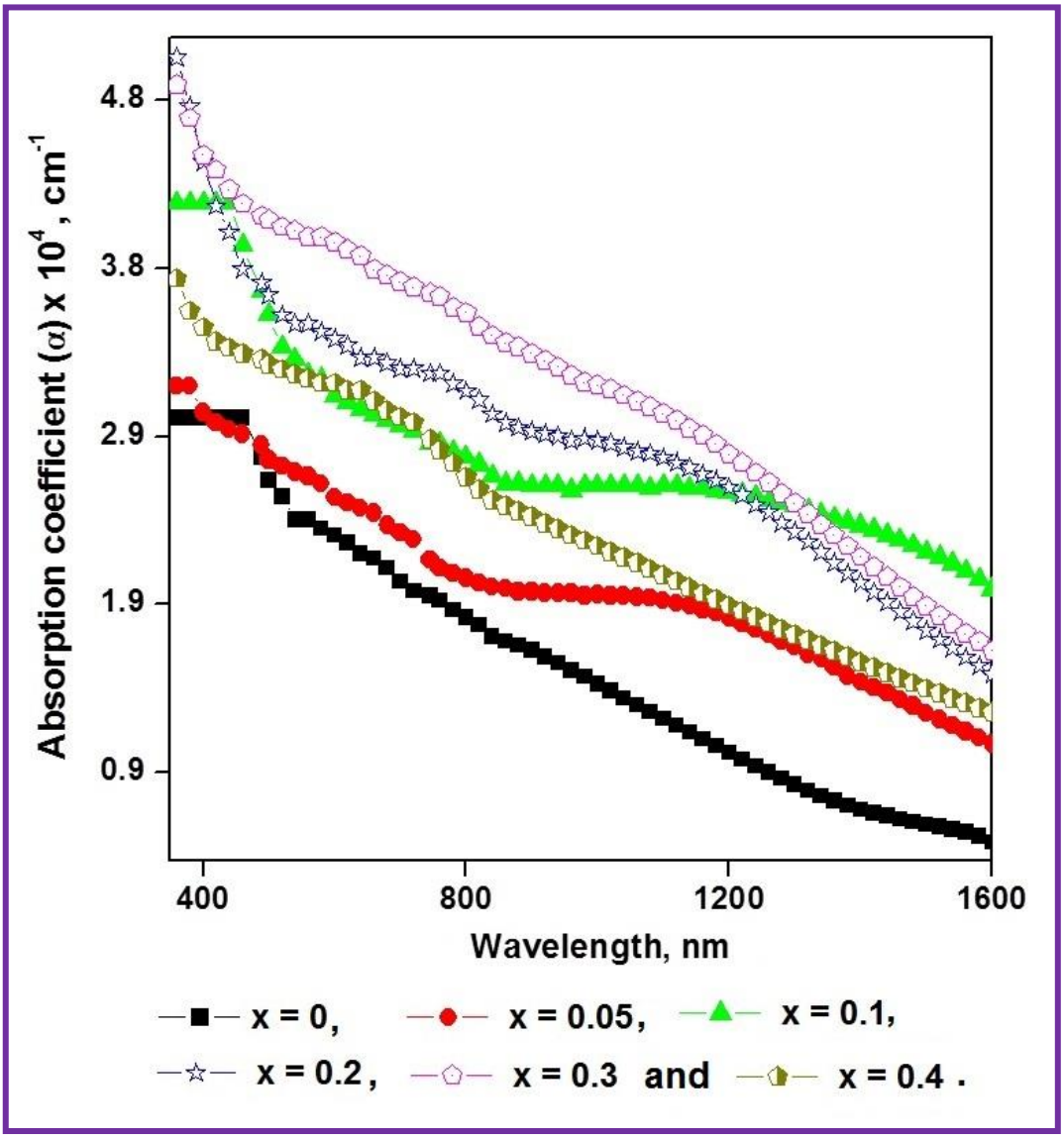

Figure 5.2. Variation of the absorption coefficient (α) vs wavelength (λ) for six representative Co-Zn-S thin film structures.

The data were systematically studied in the vicinity of the absorption edge on the basis of three-dimensional model. In semiconductors, the optical absorption spectrum is found to have three distinct regions:

i) high absorption region ($\alpha \geq 10^4\ cm^{-1}$)

ii) exponential edge region ($1 \leq \alpha \leq 10^4\,cm^{-1}$)

iii) weak absorption tail (practically zero).

At higher wavelengths, the non-linear tail absorption in the curves may be due to the transitions associated with the absorption of longer wavelength phonons [4, 25, 26]. In the high absorption region ($\alpha \geq 10^4\,cm^{-1}$), the relation between the absorption coefficient (α) and the incident photon energy ($h\nu$) can be written as [3, 4, 17]

$$(\alpha h\nu) = A\left(h\nu - E_g\right)^n \qquad \text{.....(5.1)}$$

where, h is a Planck's constant, A is a parameter that depends on the transition probability and E_g is the optical energy gap of the sample under investigation and exponent n depends on the type of transition. For direct allowed transitions, n = 1/2, for indirect allowed transitions, n = 2 and for direct forbidden transitions, n = 3/2. The values of the optical band gaps were then calculated from the best straight line fits in the $(\alpha h\nu)^2$ versus $h\nu$ plots (fig. 5.4 (a and b)) and corresponding band gaps were obtained from the extrapolation of the straight portion of the graph at $(\alpha h\nu)^2 = 0$. In our case the band gap of CoS is found to be 1.59 eV. It is also observed that the optical band gap increased from 1.59 eV to 2.50 eV as the composition parameter (x) was increased from 0 to 0.4. The variation in band gap with zinc content is found to be non-linear. The values of the band gap for different compositions are listed in table 5.1. The increase in the band gap can be ascribed to the presence of Zn^{2+} that adds additional gap states in the band gap of CoS [14-16]. The non-linear variation of the band gap is found to be due to the local non-stoichiometry, quantum size effect and large density of dislocations [3,

4, 14]. The variation in band gap with composition parameter (x) is shown in fig. 5.5. The plots of $(\alpha h\upsilon)^2$ vs $h\upsilon$ are linear in the high energy region indicating direct, band to band type, transitions.

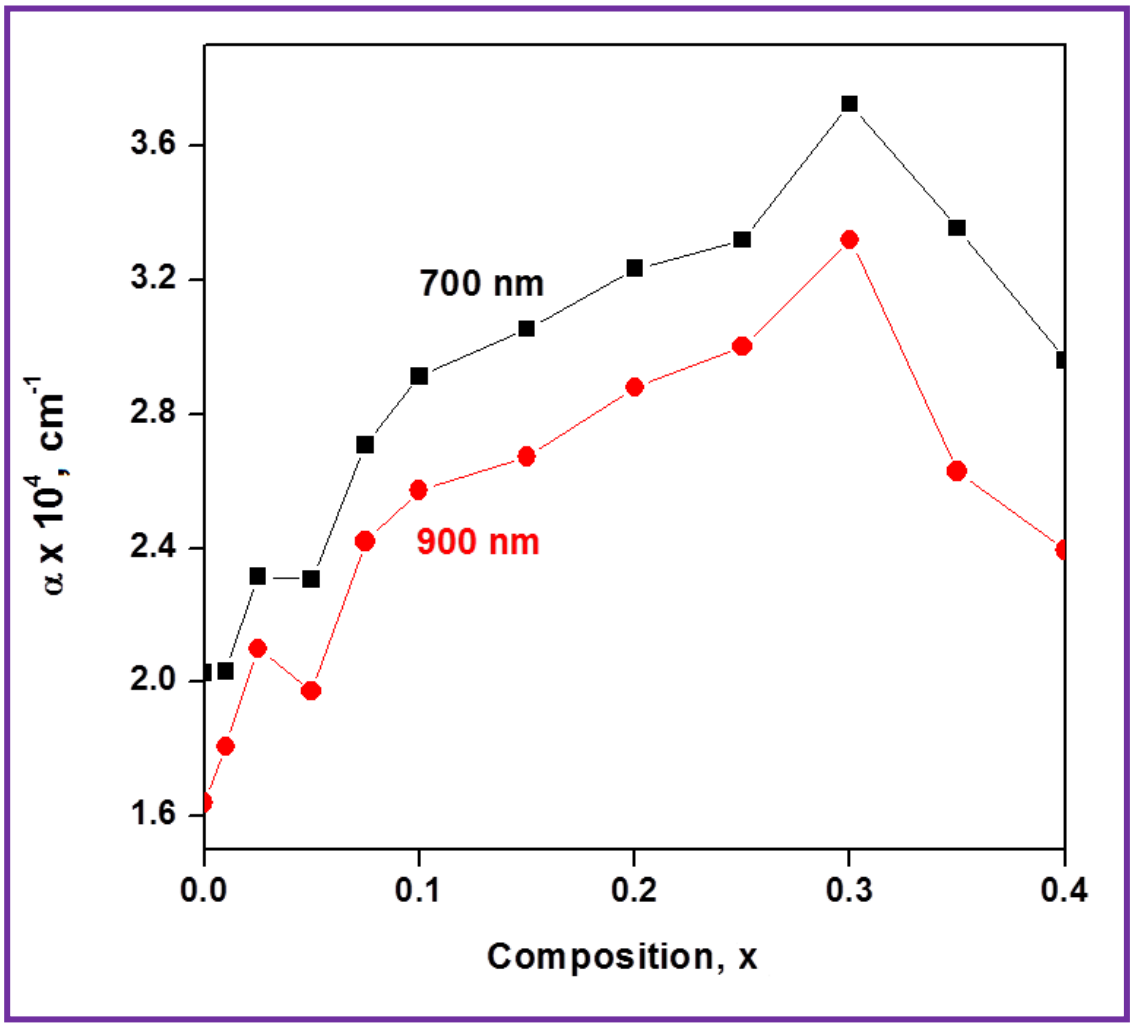

Figure 5.3. Composition dependence of the absorption coefficient (α) at 700 nm and 900 nm wavelengths.

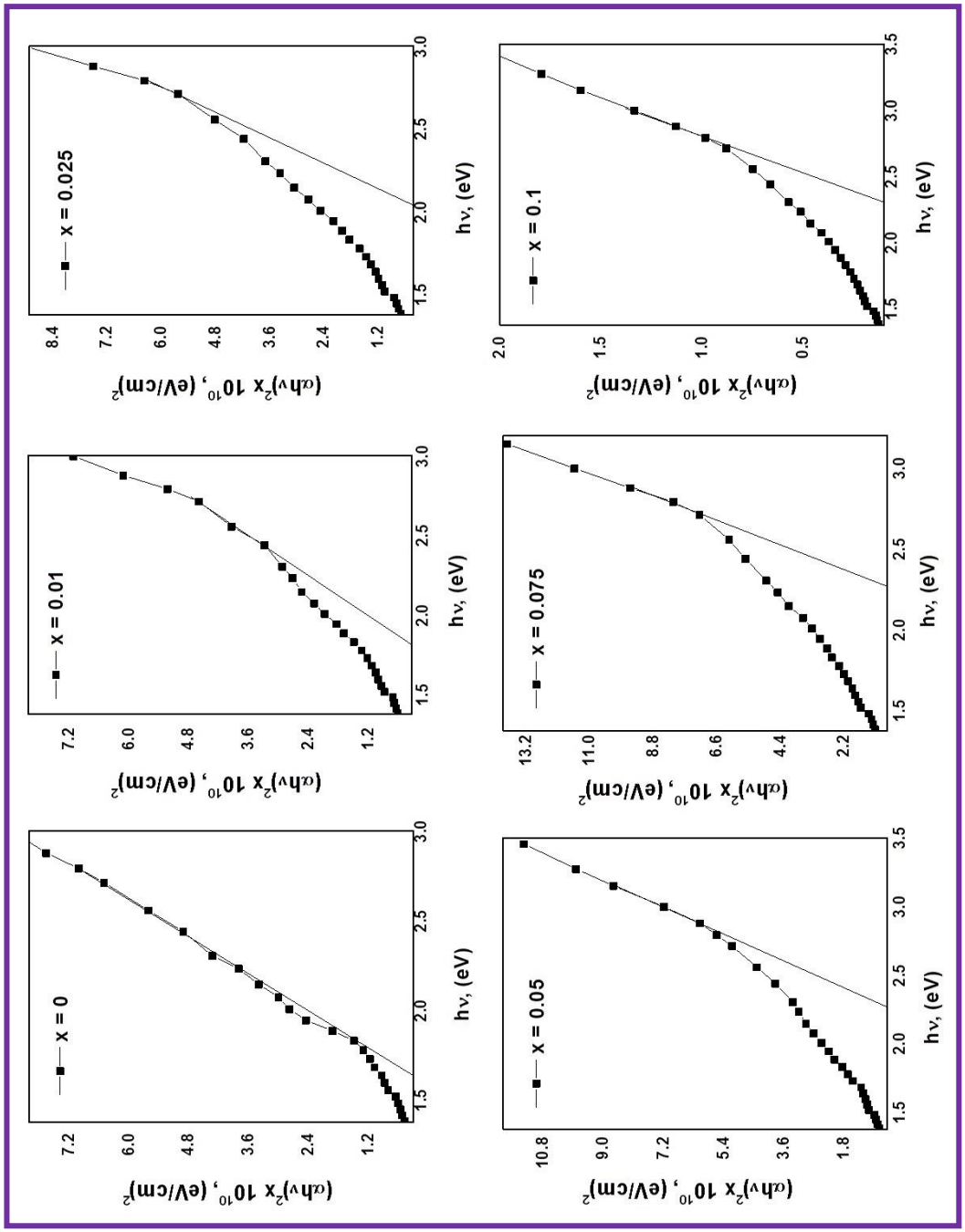

Figure 5.4 (a). $(\alpha h\nu)^2$ vs $h\nu$ plots for CoS and $Co_{1-x}Zn_xS$ ($0 \leq x \leq 0.1$) thin films.

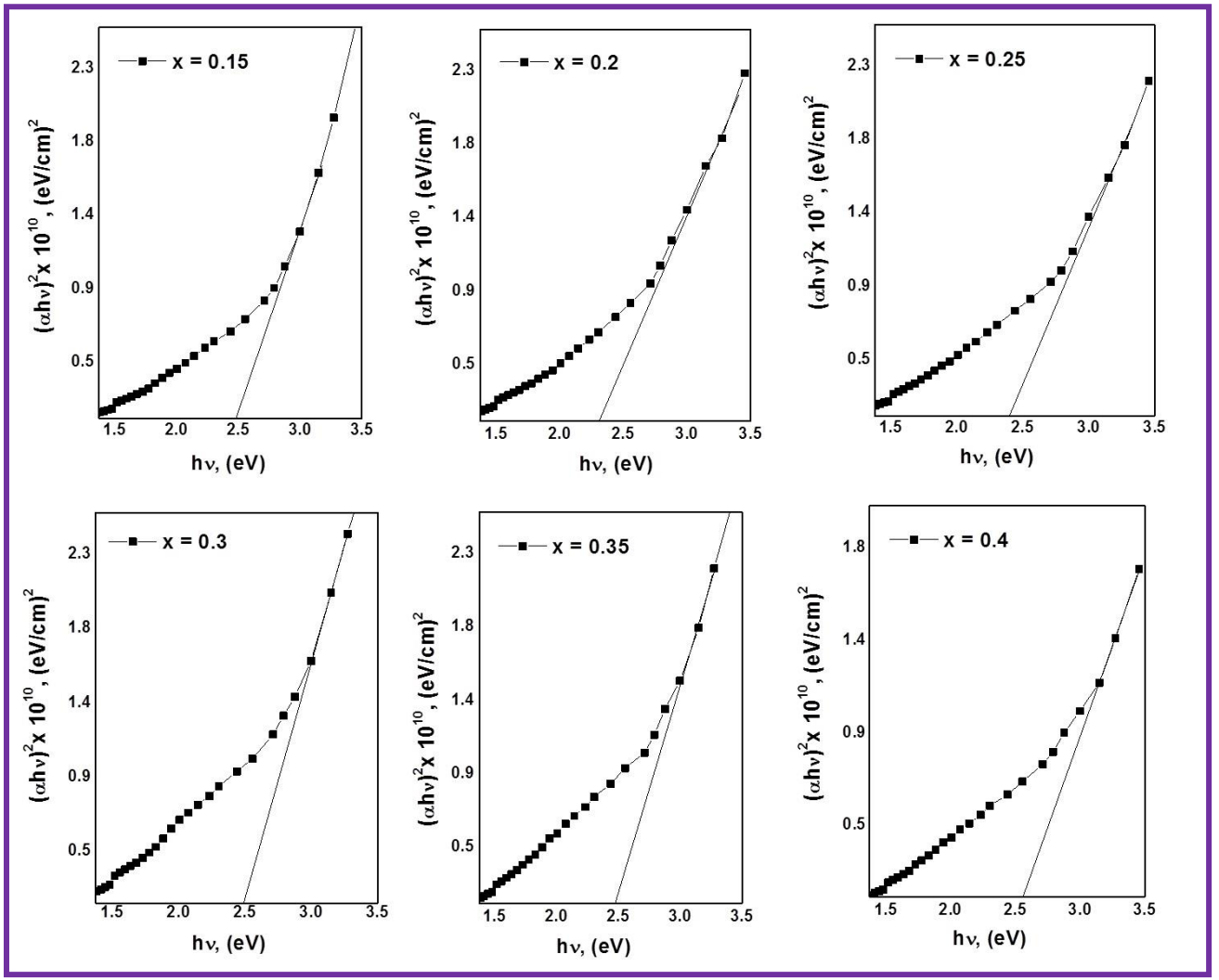

Figure 5.4 (b). $(\alpha h\nu)^2$ vs $h\nu$ plots for CoS and $Co_{1-x}Zn_xS$ ($0.15 \leq x \leq 0.4$) thin films.

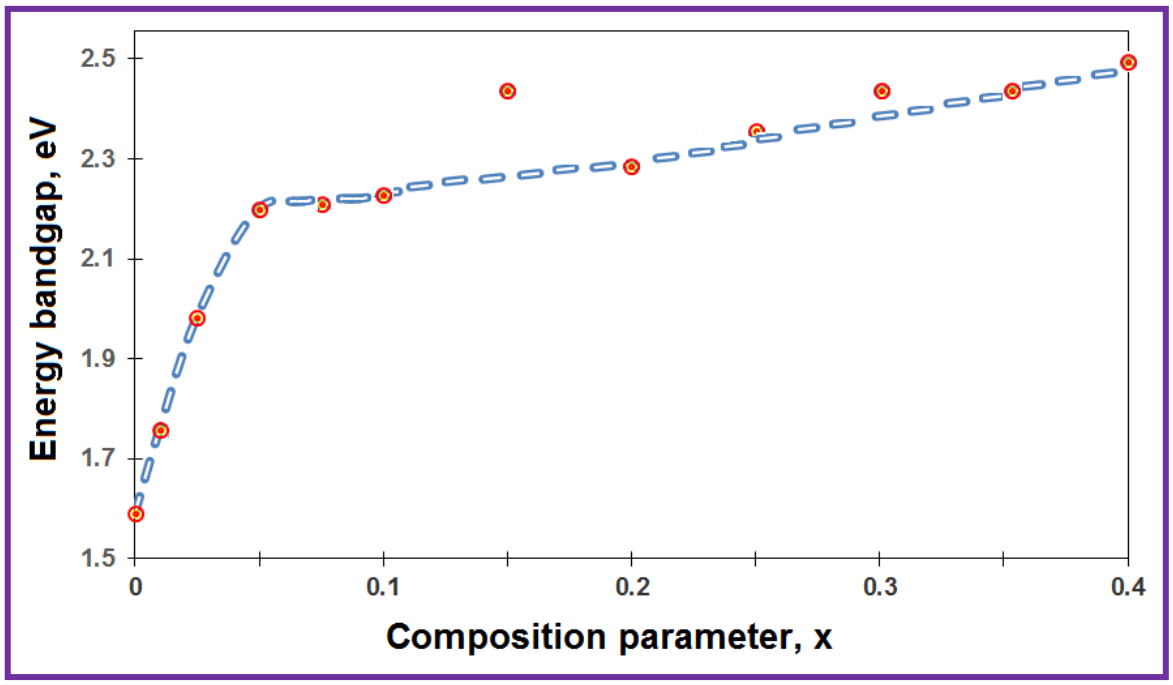

Figure 5.5. Variation in the optical band gap (Eg) with the composition parameter (x).

The mode of optical transitions in these materials was also checked. The equation can be represented as [3, 4, 17];

$$\ln(\alpha h\nu) = \ln A + 0.5\ln(h\nu - E_g)\,. \qquad \ldots\ldots (5.2)$$

For direct allowed type transitions, a plot of ln (αhυ) versus ln (hυ-Eg) should give a straight line with a slope equal to 0.5 (power factor). Figure 5.6 represents the results of the above analysis for a few of the compositions and the values of m's are listed in table 5.1.

The materials other parameters namely, E_a (opt), k, n, reflectivity (R), ε, ε", ε_0, ε_∞ and m_e^*/m_0 were then computed since they determine the optical and transport characteristics

of the material [1, 3, 4]. The optical activation energy, E_a (opt) is related to the energy band gap (E_g) and is expressed by the following relation [27-30];

$$E_{a\ (opt)} \cong \frac{E_g}{2}. \qquad \text{..... (5.3)}$$

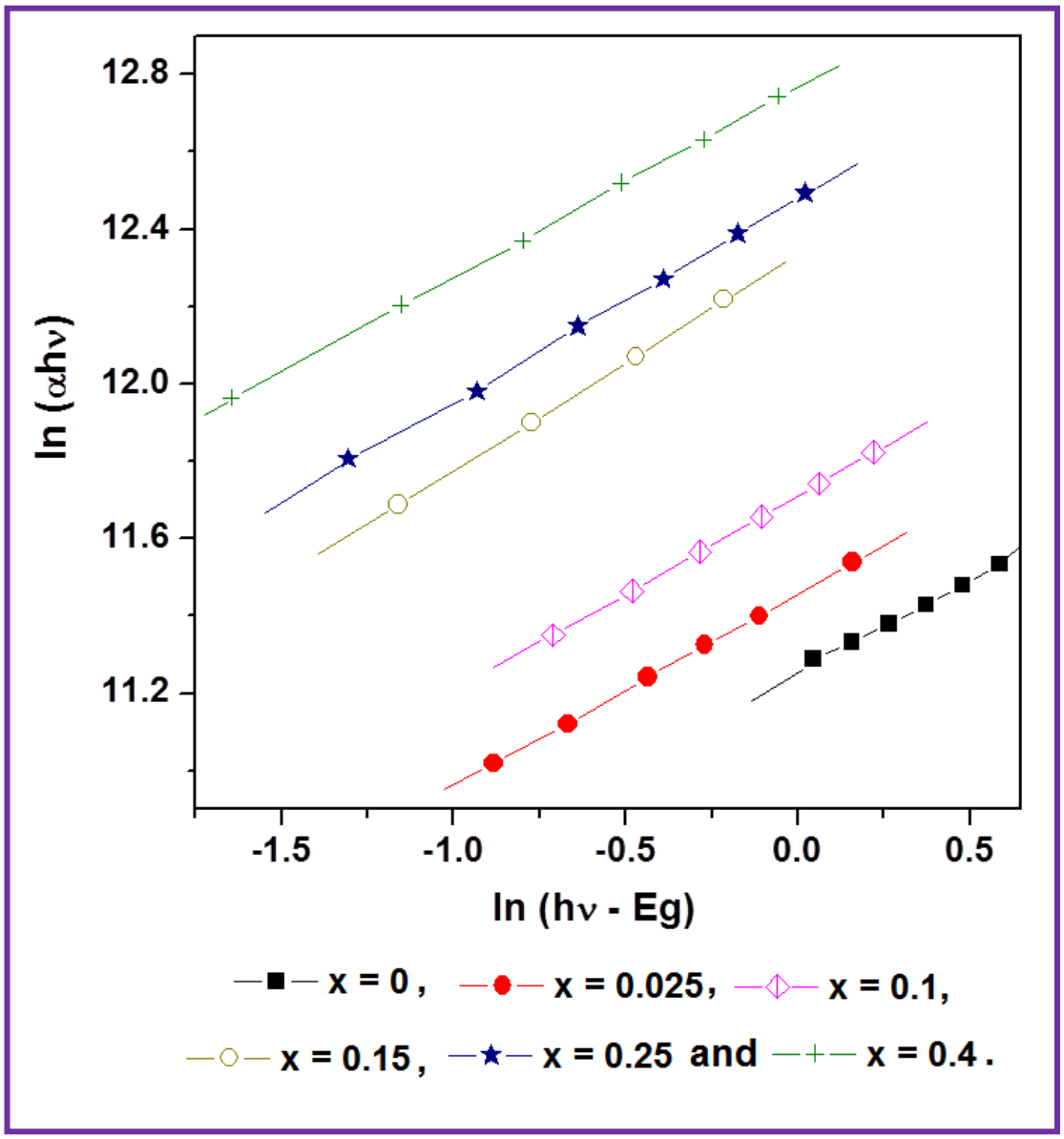

Figure 5.6. Plots of ln (αhν) vs ln (hν-Eg) for the determination of transition index.

The extinction coefficient (k) is a measure of fraction of light lost due to scattering and absorption per unit distance of the penetration medium. It can be estimated from the values of α and λ using the relation [27-30],

$$k = \frac{\alpha\lambda}{4\pi}. \qquad \text{..... (5.4)}$$

The refractive index (n) bears the following relation with the energy gap (Eg) [27-30];

$$n = 4.16 - 0.85E_g \, . \qquad \text{..... (5.5)}$$

The reflectivity (R) of the absorbing medium was calculated by the following relation;

$$R = [(n-1)^2 + k^2]/[(n+1)^2 + k^2]. \qquad \text{..... (5.6)}$$

The complex dielectric constant is a fundamental intrinsic property of the material. The real part of the dielectric constant shows how much it will slow down the speed of light in the material, whereas the imaginary part shows how a dielectric material absorbs energy from an electric field due to dipole motion. The knowledge of the real and the imaginary parts of the dielectric constant provides information about the loss factor which is the ratio of the imaginary part to the real part of the dielectric constant. The real (ε) and the imaginary (ε") parts of the dielectric constant can be estimated using the relations [27-30];

$$\varepsilon = n^2 - k^2. \qquad \text{.....(5.7)}$$

and

$$\varepsilon'' = 2nk \, . \qquad \text{.....(5.8)}$$

The static dielectric constant (ε_0) and high frequency dielectric constant (ε_∞) were also evaluated for all the film structures [27-30] using;

$$\varepsilon_0 = -33.26876 + 78.61805E_g - 45.70795E_g^2 + 8.32449E_g^3 \quad \text{.....(5.9)}$$

and

$$E_\infty = n^2 . \quad \text{.....(5.10)}$$

The electron effective masses m_e^*/m_0 for the different films were then determined from its dependence on the energy gap as [27-30];

$$m_e^*/m_0 = 5.17004 - 7.4669E_g + 3.63286E_g^2 - 0.57525E_g^3 . \quad \text{.....(5.11)}$$

5.3.2. The electrical conductivity studies

The electrical transport properties play an important role in deciding the quality as well as application of the thin films in semiconductor devices. These properties are strongly influenced by their structural characteristics, purity, nature and concentration of the impurities [1, 3, 4, 31, 32]. At low temperature, thermal energy is just sufficient to allow migration of the carriers into the vacancies already present in the materials, whereas at high temperature, thermal energy is sufficient to create vacancies that are responsible for movement of the charge carriers. The parameters of interest in this study are the electrical conductivity, type of the conductivity (n or p), mobility and carrier concentration. The contact method is most widely used method for the measurement of the electrical conductivity. The method includes two probes and/ or four probes. The two probe method is simple, easy to use and useful for high resistive thin films. In this method, a constant dc voltage V was applied between the two fixed positions on the surface of the thin film. The current passing through a sample of known dimensions is

measured with an appropriate current meter. The dark dc electrical conductivities of all the samples were measured using this two probe method in the temperature range from 300 K to 550 K. The specific conductance of CoS at room temperature was found to be of the order of $\approx 10^{-6}(\Omega.cm)^{-1}$ and it decreased with the film composition parameter, x. Further, the conductivity of the samples increased with increase in temperature showing Arrhenius behaviour of the films. The plots of log σ vs1000/T are shown in fig.5.7 for seven representative samples. There are two distinct linear regions indicating presence of two-conduction mechanisms; the low temperature extrinsic and high temperature intrinsic [8, 9, 11, 12, 33]. The low temperature range (300 K – 350 K) is characterized by the small slope. Whereas, high temperature range is characterized by a large slope. In both the regions, electrical conductivity is found to be decreased with increase in Zn-content in the film; the variations are larger for small range of composition ($0 \leq x \leq 0.15$) and thereafter they are not much significant. This is analogous to our earlier observations on CdS:Zn [5] and CdSe:Zn thin films [5 (a)]. The decrease in electrical conductivity, at this moment, can be attributed to the increased effective band gap of the material that reduces the transport of charge carriers from valance to the conduction band. The carrier mobility may also be reduced causing reduction in the electrical conduction (this will form the later part of the studies).

In general, the transport behaviour of the CoS and $Co_{1-x}Zn_xS$ thin films is analogous to the behaviour of polycrystalline semiconducting thin films and therefore, the type of conduction mechanism was studied in both temperature regions. It appeared that high

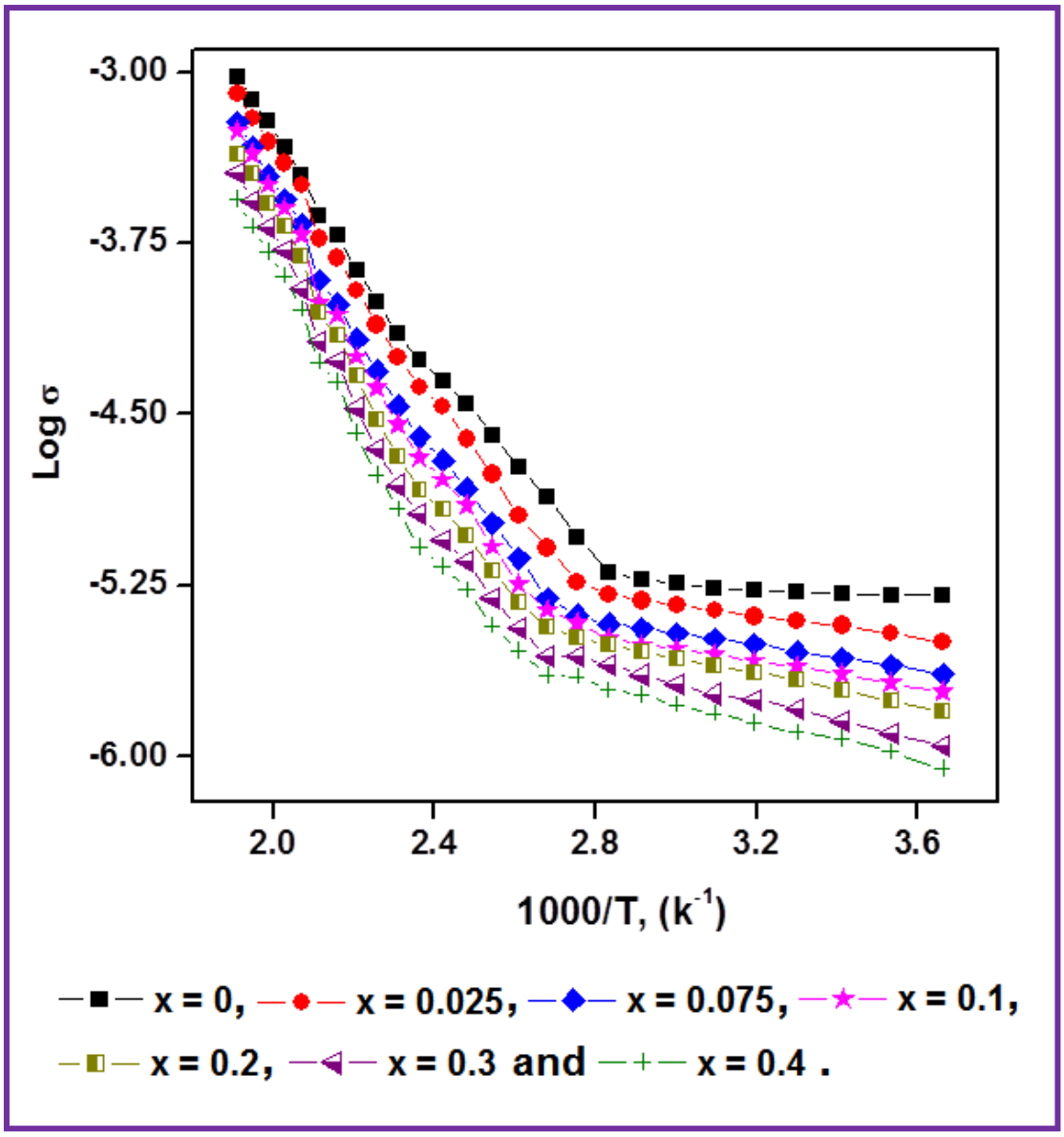

Figure 5.7. Variation of an electrical conductivity with working temperature for few of the representative Co-Zn-S thin films.

temperature region is characterized by a grain boundary scattering limited conduction mechanism as evidenced by the plots of log $(\sigma T)^{1/2}$ Vs. $100/T^{1/4}$ (fig. 5.8) [3, 18, 19, 33]. The plots are liner showing that, the electrical conduction in this range of temperature is affected by the grain boundaries associated with the material and that the mechanism is

attributed to the thermal excitations of the charge carriers across the potential barrier at grain boundaries. The experimental data in this range of temperature (T >350 K) can be fitted to an Arrhenius behaviour as [3, 18, 19, 33],

$$\sigma = \sigma_0 \left[\exp\left(-\frac{E_a}{kT} \right) \right] \qquad \text{.....(5.12)}$$

where, E_a is the activation energy and T is the absolute temperature. Values of E_a's were evaluated from this plot and are given in table 5.2. Low-temperature (T < 350 K) conduction involves tunneling between the localized states [18-20, 34] and across the barrier called variable range hopping conduction. This is a low activation energy process. The data can be fitted to;

$$\sigma = \sigma_{n0} \exp\left(\frac{-T_0}{T} \right)^{1/4} \qquad \text{.....(5.13)}$$

where, the value of T_o is related to the degree of disorder of the semiconductor. The above equation can be rearranged as log $(\sigma T^{1/2}) \alpha T^{-1/4}$ [18, 19, 34]. The plots are linear showing that equation (5.13) holds good in the low temperature zone. This confirms that the dominant mechanism in the low temperature range is the variable range hopping conduction mechanism. The localized states responsible for this conduction process are the direct consequence of the imperfections associated with the polycrystalline thin films [7-9, 11, 35, 36]. These imperfections may, probably, be generated in our samples due to incomplete atomic bonding at the grain boundaries and partly due to the stoichiometric deviation (in our case stoichiometric deviation is large). The activation energies were then determined and are tabulated in table 5.2.

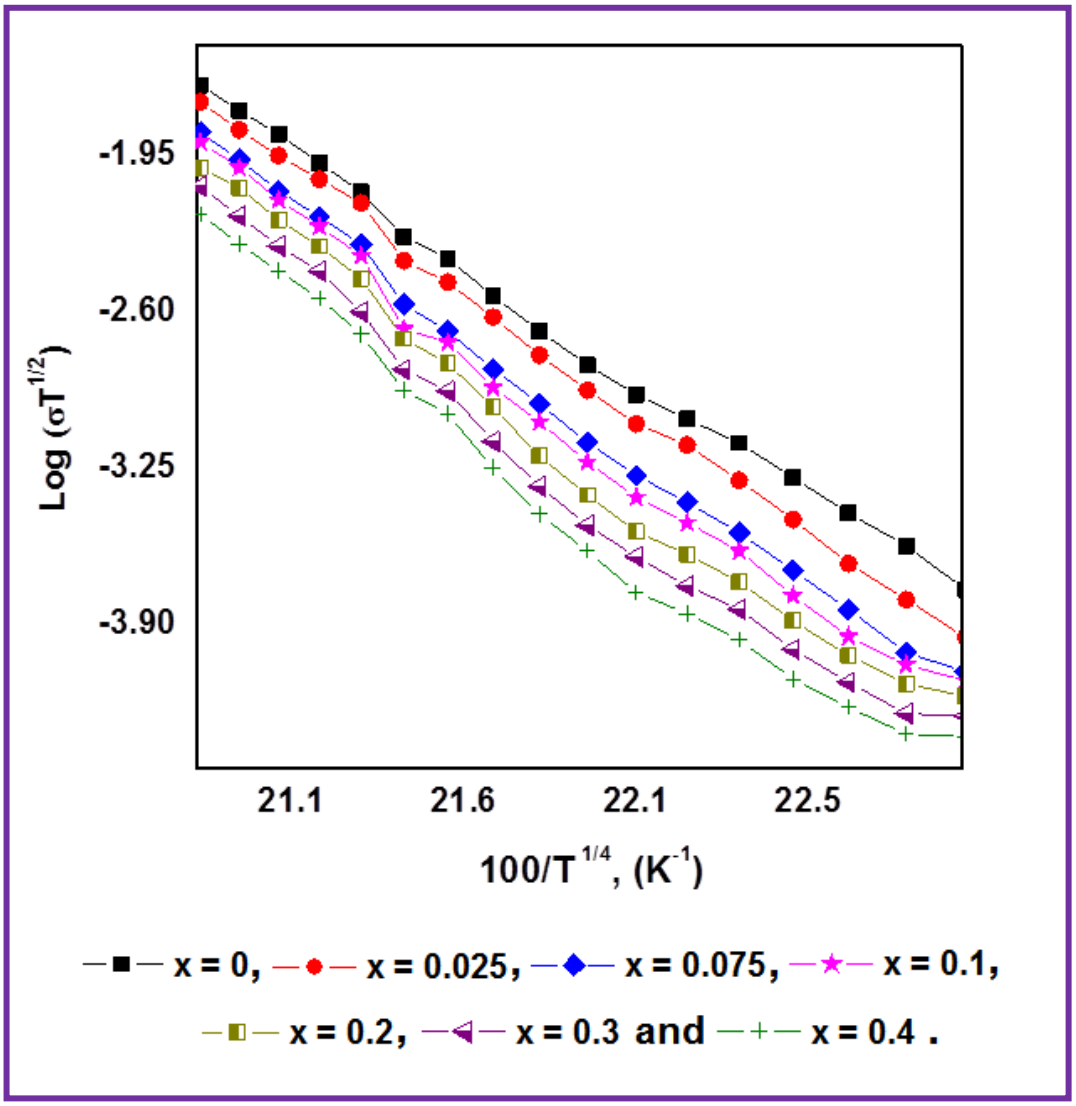

Figure 5.8. Plots of log ($\sigma T^{1/2}$) versus $100/T^{1/4}$ for seven representative CoS and $Co_{1-x}Zn_xS$ thin films.

It is seen that, in both the cases, the activation energies increased with increase in Zn^{2+} concentration in CoS. The increase in activation energy may be partly ascribed to the decreased carrier concentration, which upturns the height of the potential barrier between the crystallites composing the films. The acceptor levels are produced below the bottom of the conduction band with $A_c = 2E_{a\sigma}$. The A_c's are also documented in

table 5.2. The composition dependence of an electrical conductivity was also examined at 473K and 503 K and is shown in fig. 5.9.

From the fig. 5.9, it is seen that the electrical conductivity decreased initially rapidly up to a value of x = 0.1 and then remained almost constant for higher values of x. The dependence of σ on film composition (x) can be explained qualitatively on the basis of the observed compositional and structural studies. The EDS studies showed substitution of Co^{2+} by Zn^{2+}. When the Zn-content in the bath was increased, Zn-content in the film also increased. A decrease in electrical conductivity has been observed with an increase in zinc content in the film. A considerable amount of disorder may be generated in the films due to the substitution of Co^{2+} by Zn^{2+}; the substitution being dominant mechanism. This is true upto a value of x equal to 0.1. At high concentration of Zn (x > 0.1) in CoS, Zn^{2+} may prefer to form ZnS rather than to replace Co^{2+}. Therefore conductivity of the sample is more or less controlled by the conductivity of CoS and ZnS as these phases have been found to be detected in the XRD studies. With increasing Zn-content in CoS, it is expected that the lattice disorder would increase, altering the crystallography of the material.

Hence variations in the electrical conductivity of $Co_{1-x}Zn_xS$ thin films can be correlated, at this moment, to the variations in the band gap and the crystallographic parameters (d, a and c) [36]. Fig 5.10 depicts a correlation/ comparison of lattice parameters (a and c) and electrical conductivity (σ) as a function of the film composition (x). It is observed that both a and c went an increasing with increasing content of Zn^{2+} in CoS, thus

transforming the structure into loosely packed structure that decreases the electrical conductivity owing to the reduced number of atoms in a cell. These variations are so small that they can be a best fit to the variations in σ at higher concentration of Zn in CoS. The second plausible reason for the decrease of electrical conductivity that we propose is that, at high concentration of Zn^{2+} in CoS, the rate of substitution of Co^{2+} by Zn^{2+} is initially higher and goes on decreasing as the time passes and finally becomes practically zero. The rest of the Zn^{2+} atoms, then adjust themselves at the interstitial sites causing increased charge trapping centers that increases the intergrain barrier potential and hence reduces the electrical conduction.

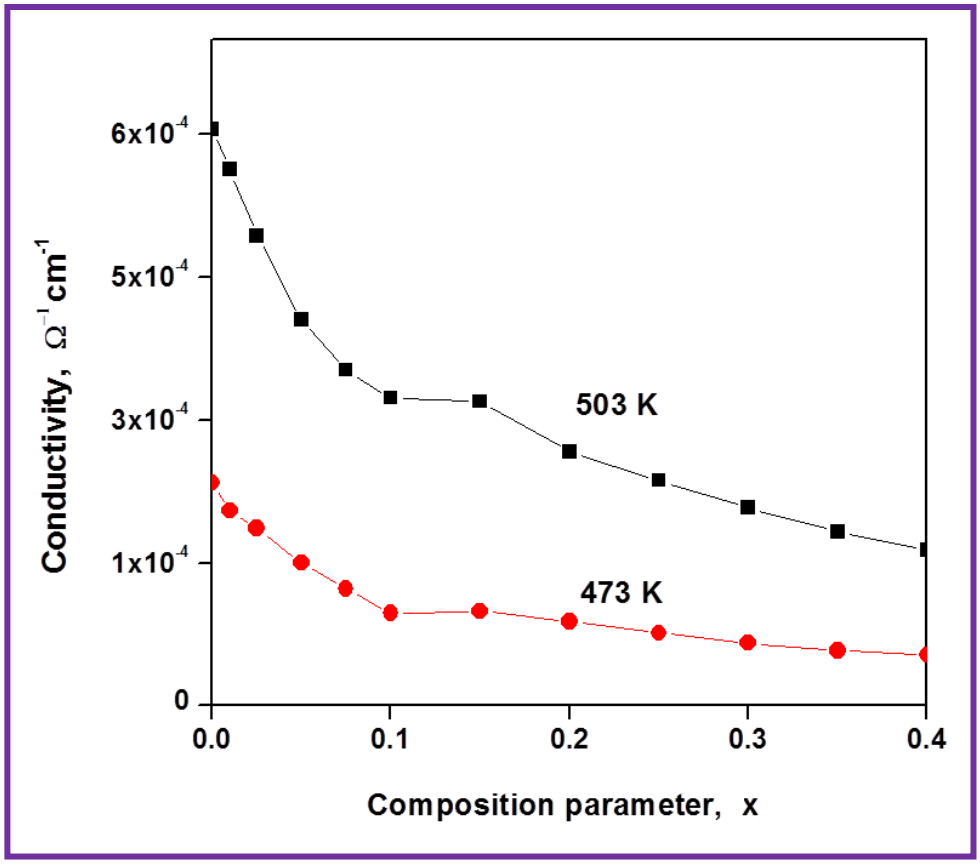

Figure 5.9. Variation in electrical conductivity (σ) with the film composition parameter (x).

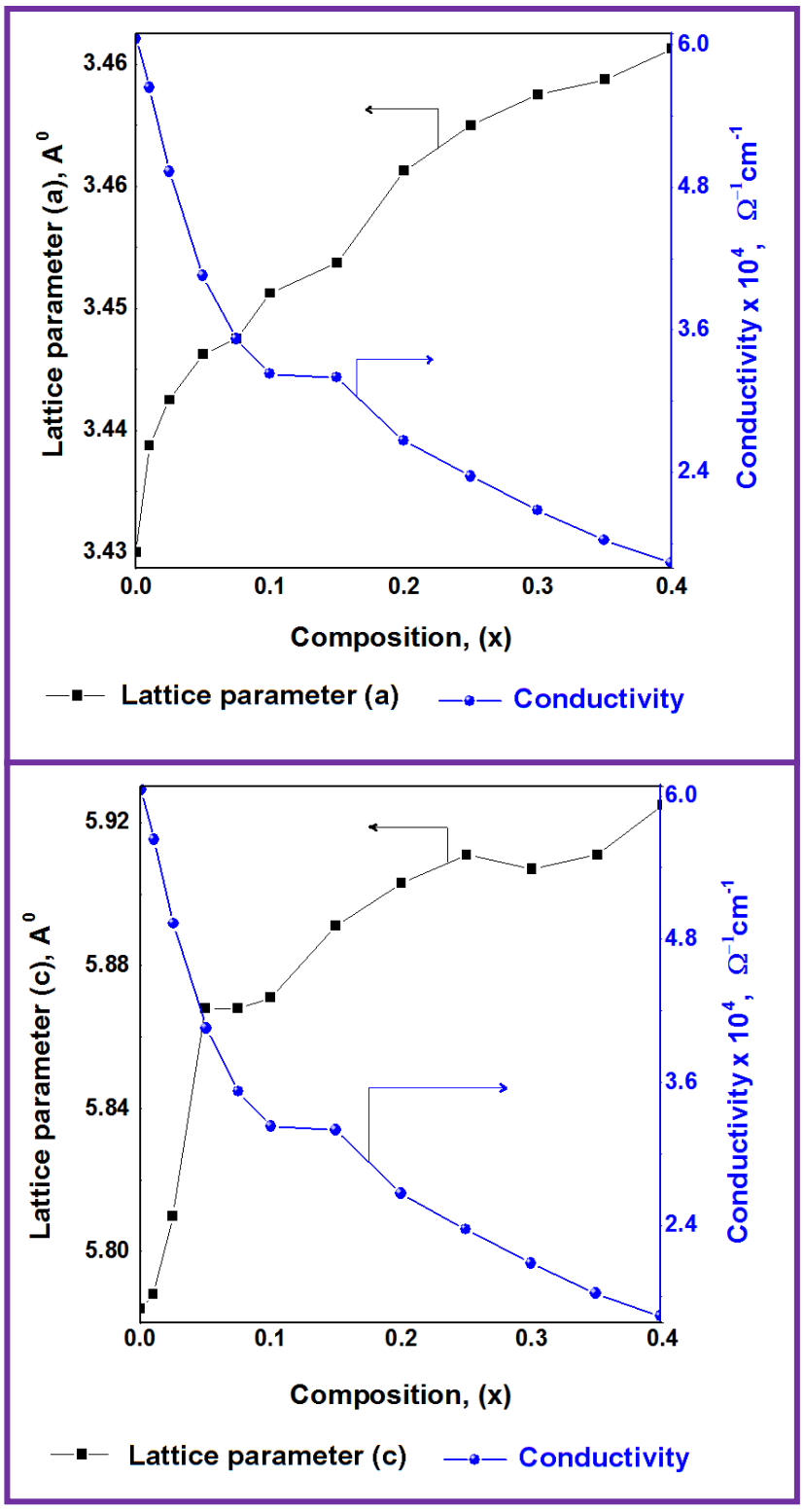

Figure 5.10. Plots depicting correlation between lattice parameters (a and c) and conductivity over the whole range of the composition ($0 \leq x \leq 0.4$).

5.3.3. Thermo-power studies

In thermoelectric power measurements, the open circuit thermo-voltage generated by the samples, when a temperature gradient is applied across length of the samples was measured. The thermoelectric power is negative for n-type semiconductor and positive for p-type semiconductor: a fact often used to determine the conduction type of a semiconductor. The thermoelectric power can also be used to determine position of the Fermi level relative to the band edges. The thermally generated voltage is directly proportional to the temperature difference created across the semiconductor. The carrier density and mobility can then be determined from thermo-emf measurements. From the polarity of thermovoltage (negative or positive), one can easily determine the sign of the predominant charge carriers and hence the type of a semiconductor (n or p-type). In our study, all the films showed n- type conductivity. Thermoelectric power measurements of all the films exhibited similar behaviour with increasing temperature. The increase in thermoelectric power with temperature suggests degenerative nature of the films [9, 11, 19, 20, 37]. The temperature dependence of thermoelectric power is shown in fig. 5.11. The TEP dependence is almost constant at low temperature region (upto 375 K) whereas it deviated at high temperature. The temperature dependence of thermoelectric power is given by [36, 37];

$$P = \left(-K/e\right)\left[A + \ln\left\{2\left(2\pi m_d * kT\right)^{3/2} / nh^3\right\}\right] \qquad \text{.....(5.14)}$$

where, A is a thermoelectric factor which depends on the various scattering mechanisms and other terms have their usual significance.

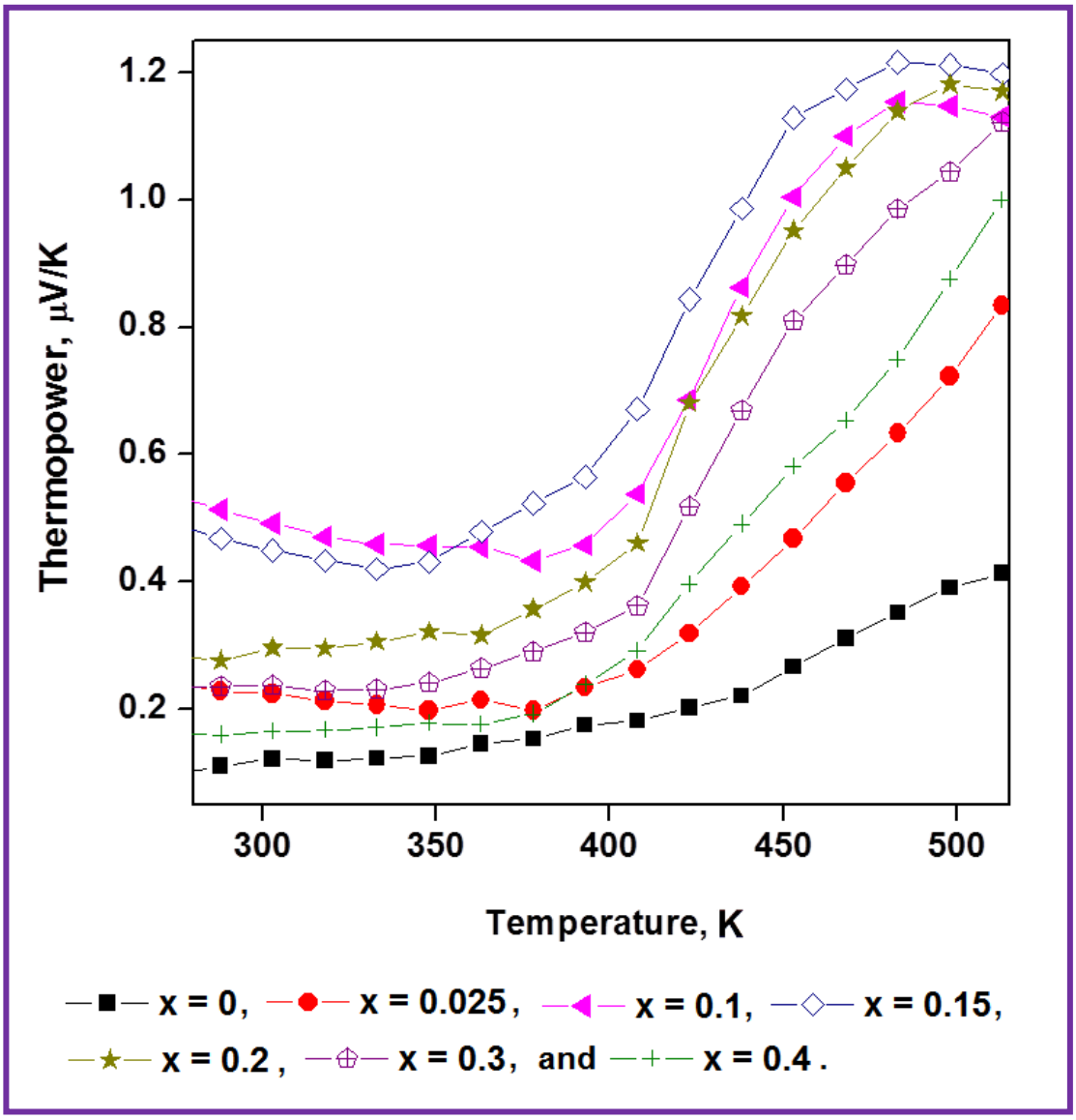

Figure 5.11. Plots of variation in thermoelectric power with working temperature for CoS and $Co_{1-x}Zn_xS$ thin films.

The composition dependence of thermopower is represented in fig. 5.12. It is seen that thermoelectric power is increased as composition parameter (x) is increased from 0 to 0.2 and then remained almost constant with minor downfall.

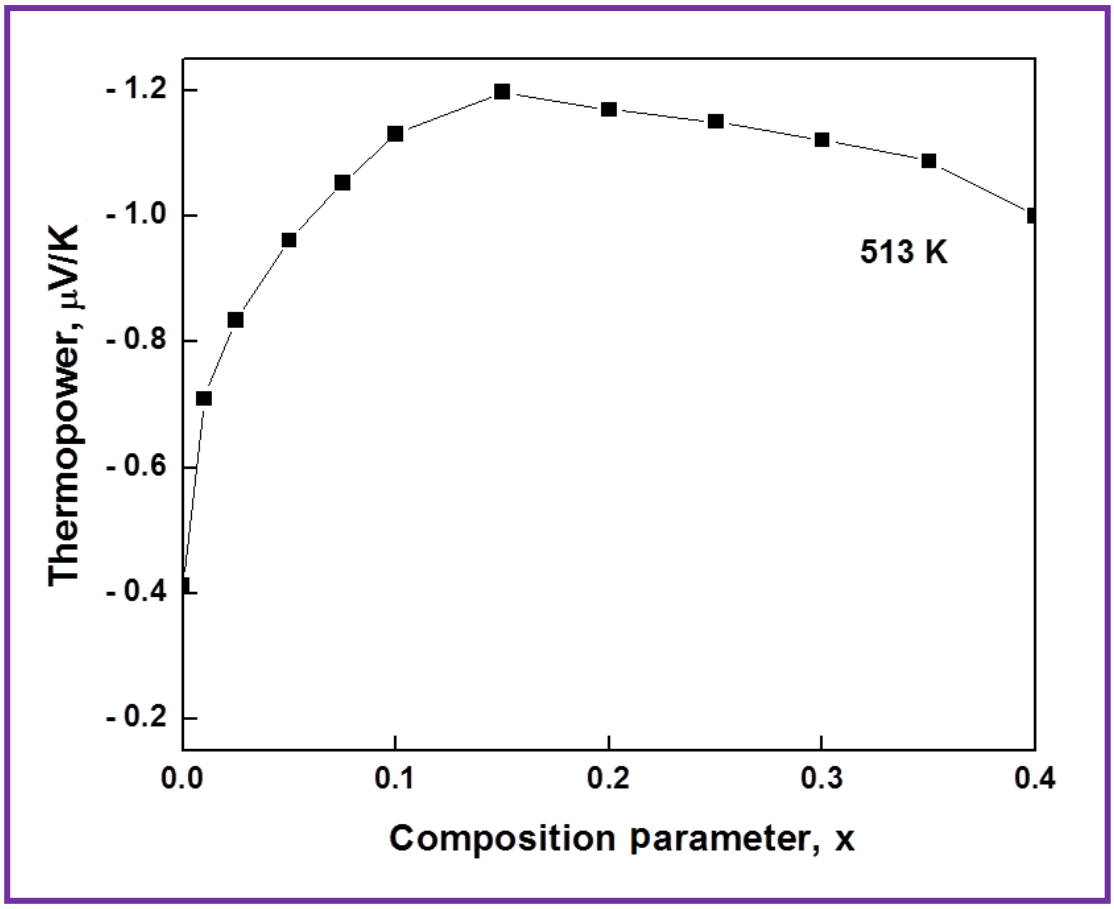

Figure 5.12. Variation in thermoelectric power with the Zn concentration in CoS and $Co_{1-x}Zn_xS$ films.

In order to have clear understanding of the conduction mechanism, attempts were also made to measure the carrier mobility (μ) and carrier concentration (n) as a function of the working temperature and composition. Equation (5.14) can be solved and rearranged for n and the temperature dependence of the carrier concentration becomes:

$$\log n = \tfrac{3}{2}\log T - 0.005P + 15.7198 . \qquad \text{.....(5.15)}$$

The carrier mobilities and densities were then calculated at different temperatures using the relation;

$$\mu = \sigma / ne . \qquad \text{.....(5.16)}$$

The plots of carrier density and mobility against the composition are shown in figs. 5.13 and 5.14, respectively. As the composition parameter (x) is increased, the carrier concentration and mobility are found to be decreased. However, both carrier concentration and mobility are found to be increased as the temperature is increased.

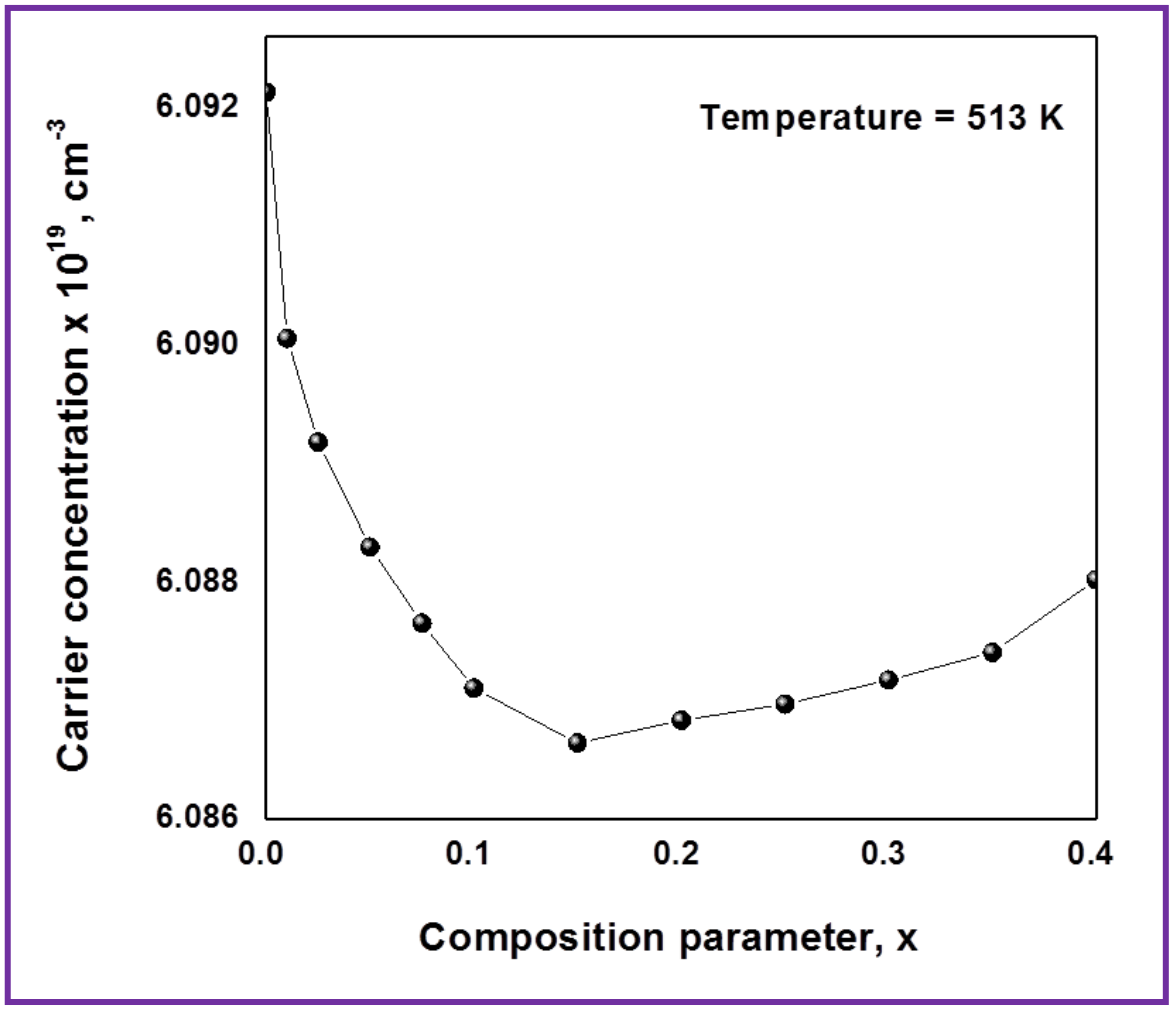

Figure 5.13. Variation in carrier concentration (n) with the film composition parameter (x).

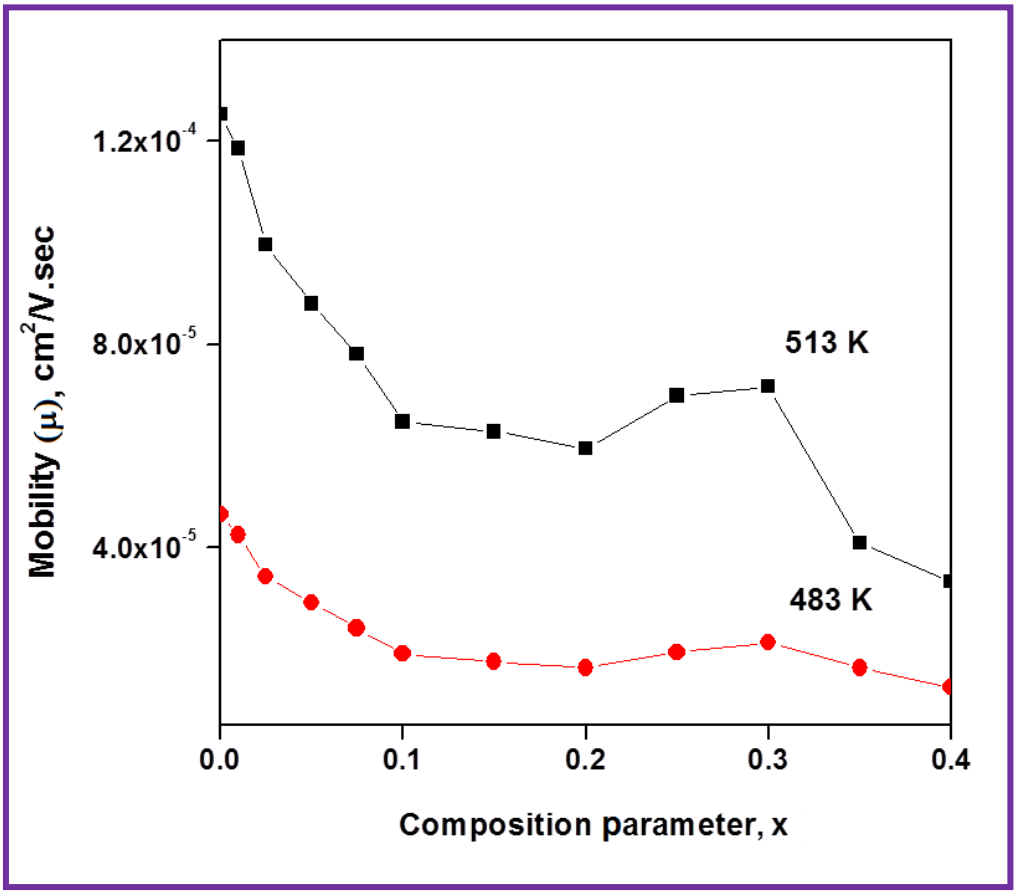

Figure 5.14. Variation in mobility (μ) with Zn concentration in CoS and $Co_{1-x}Zn_xS$ thin films.

The dependence of carrier mobility on temperature was also studied and suggests the possibility of scattering mechanism associated with the inter-grain barrier potential [36-38]. The temperature dependent grain boundary mobility is related to the grain boundary potential as;

$$\mu = \mu_0 \exp\left(-\Phi_B / kT\right) \qquad \text{.....(5.17)}$$

where, Φ_B is the height of the potential barrier at the grain boundary in eV, μ_0 is the pre-exponential factor, which on the assumption that current over the barrier flows by the

thermionic emission that depends on the grain size D and effective mass of the electron as;

$$\mu_0 = eD/(2mkT)^{1/2} \quad \text{..... (5.18)}$$

Fig. 5.15 shows plot of log ($\mu T^{1/2}$) vs 1000/T for six typical CoS and $Co_{1-x}Zn_xS$ samples. The plots are almost straight line in the region of interest thus, indicate presence of grain boundary scattering limited conduction mechanism [20, 36-38].

The grain boundary potentials (Φ_B) were then determined from the linear regions of these plots and are tabulated in table 5.2. It is seen that the inter-crystallite barrier potential increased up to x = 0.15 and then decreased a little. The increase in carrier mobility with temperature prevails the possibility of scattering mechanism associated with the inter-grain barrier potential, whereas mobility is reduced ominously with the film composition x (fig. 5.15). This also suggests why conductivity variations are not as per our expectation when Zn^{2+} is incorporated in CoS, although Zn^{2+} is more metallic than Co^{2+} and looses outermost electrons easily than Co^{2+}.

5.3.4. The photoconductivity studies

Recently, a great deal of attention has been paid to the photoconductivity studies due to its potential implications in photonics devices, such as optical switches, holographic data storage, etc [39-41]. In semiconductors, photoconductivity generally arises due to the generation of electron–hole pairs as a result of interaction of photons with bound electrons in a lattice atom [40]. Variation of photocurrent as a function of various parameters e.g. intensity of light, applied field, working temperature etc, give a useful

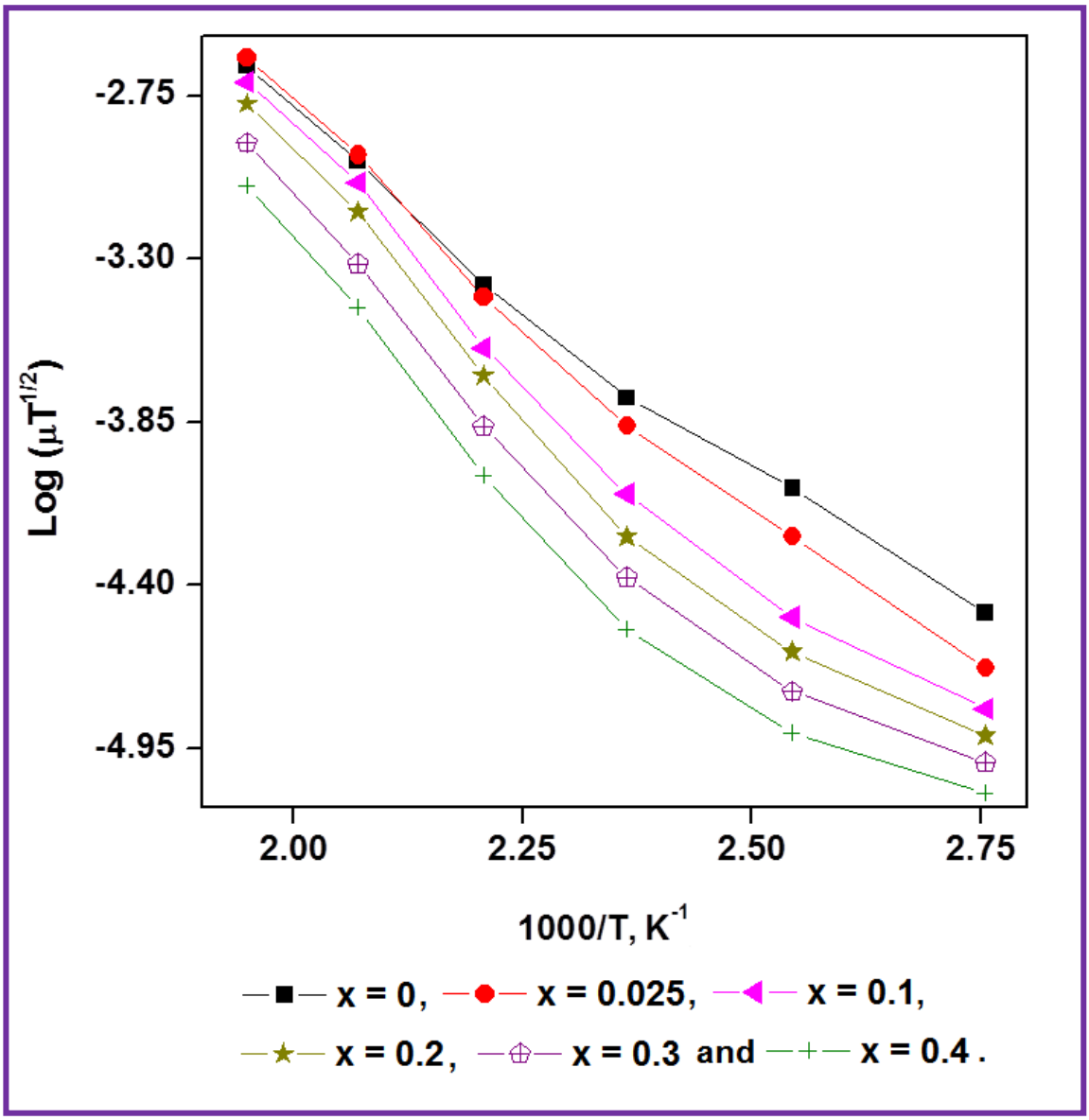

Figure 5.15. Plots of log ($\mu T^{1/2}$) versus 1000/T for six representative CoS and $Co_{1-x}Zn_xS$ thin film samples.

information regarding the materials properties [41]. Rise and decay curves are governed by the trapping states and recombination centers lying in the band gap and can be used to understand the nature and distribution of traps and recombination centers [41]. The principle of photoconductivity measurements is simple. It consists of measurements of variations in the resistivity induced by the illumination of the sample. The intensity (I) of the incident light at a distance x from the surface inside the semiconductor is related to the absorption coefficient (α) according to the law $I = I_0 e^{-\alpha x}$. The conductivity (σ) gets modified, if the absorption is due to the excitation of the free carriers and is given by;

$$\sigma = ne\mu. \qquad \text{…..(5.19)}$$

Under illumination, a change in conductivity occurs and hence the new conductivity $(\sigma + \Delta\sigma)$ can be expressed as;

$$(\sigma + \Delta\sigma) = (n + \Delta n)e(\mu + \Delta\mu). \qquad \text{…..(5.20)}$$

From this, it can be seen that there are two distinct methods of affecting the conductivity of the sample; changing the mobility of the carriers or changing the carrier density [42, 43]. From the simple semiconductor theory, illuminating a sample with light will produce a change in the carrier density if the energies of the incident photons are equal to the energy gap of the material. In this case an electron is promoted from the valence band to the conduction band and a hole is formed in its place. The change in mobility can be caused by a number of different mechanisms. If the scattering is dominated by the charged impurities, the mobility can be affected by either changing the density of impurities in the material or by changing their scattering cross-section. The

photoconductivity studies as a function of the wavelength for CoS and $Co_{1-x}Zn_xS$ samples were done on homemade setup. At room temperature, photocurrents of the CoS and $Co_{1-x}Zn_xS$ samples were measured at different wavelengths (300 nm - 1400 nm) using the filters of different colours at constant illumination intensity (5 mW/cm^2). It was observed that photocurrent increased with wavelength, peaks at a particular wavelength and then decreased for further higher wavelengths. The materials spectral sensitivities were then calculated using the relation;

$$S = \frac{(\sigma_L - \sigma_d)}{\sigma_d} \qquad \text{.....(5.21)}$$

where, σ_d is the electrical conductivity in dark and σ_L is in light. The variation in spectral sensitivity with the incident wavelength for various CoS and $Co_{1-x}Zn_xS$ ($0 \leq x \leq 0.4$) samples is shown in fig.5.16 whereas fig. 5.17 shows composition dependence of the spectral sensitivity. It is observed that sensitivity decreased gradually with increase in x up to 0.075 and thereafter it increased for x = 0.1 and then decreased. These results are not in consonance with our earlier reports.

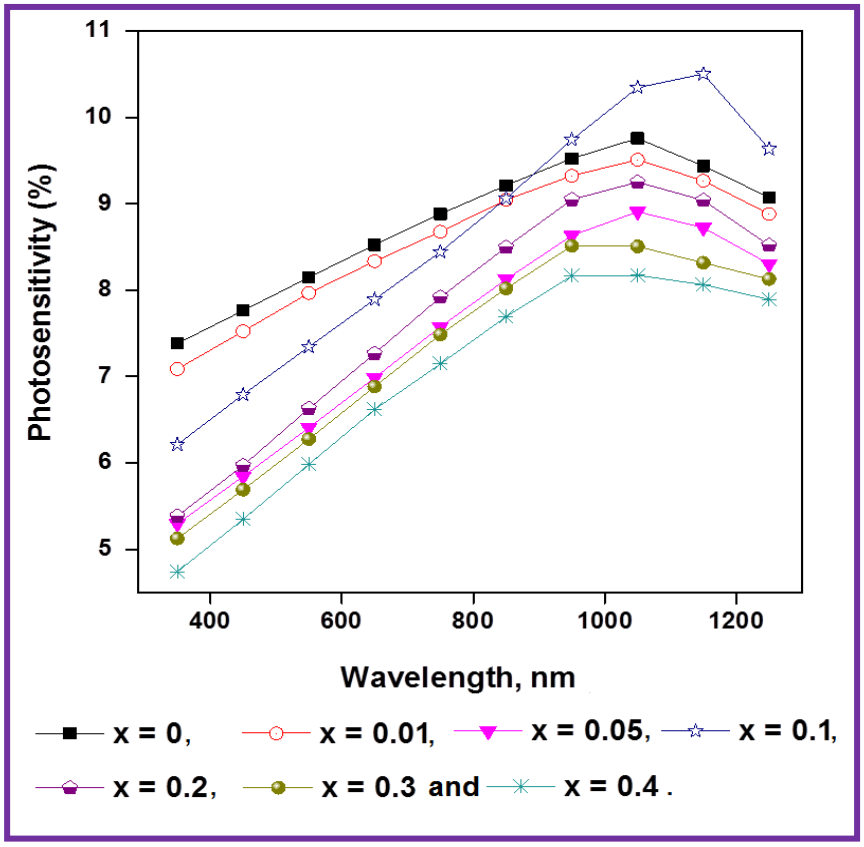

Figure 5.16. The variation in photosensitivity for CoS and various $Co_{1-x}Zn_xS$ thin films.

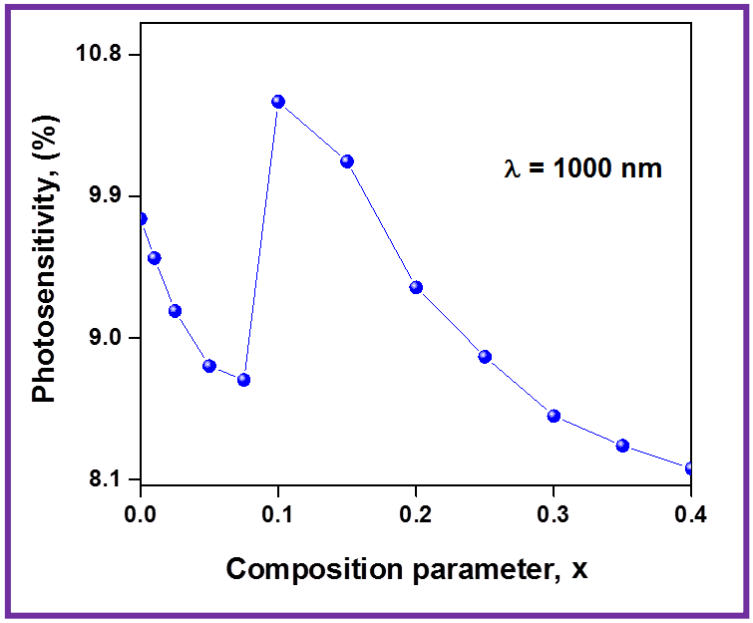

Figure 5.17. The variation in photosensitivity as a function of the film composition (x).

5.4. Conclusions

- The $Co_{1-x}Zn_xS$ films are highly absorptive and show direct type of transitions. As the composition parameter is increased, the absorption edge shifts towards smaller wavelength. The band gap increased from 1.59 eV to 2.50 eV as the composition parameter is increased.
- The electrical conductivity is found to be of the order of 10^{-6} $(\Omega.cm)^{-1}$. There are two distinct linear regions indicating the presence of two-conduction mechanisms; the low temperature extrinsic and high temperature intrinsic. Electrical conductivity is decreased with the film composition parameter increased. All the samples are of the n-type.

Table 5.1. Some optical characteristics of the CoS and $Co_{1-x}Zn_XS$ ($0 \leq x \leq 0.4$) thin films.

Composition (x)	α x 10^4, cm^{-1} λ = 700 nm	Band gap (Eg) eV	Power Factor (m)	$E_{a(opt)}$ eV	Extinction Coefficient (k)	Refractive Index (n)	Reflectivity R	Real Dielectric Constant (ε)	Imaginary Dielectric Constant (ε'')	Static Dielectric Constant (ε0)	High Frequency Dielectric Constant (ε_∞)	Electron Effective Masses (me*/m0)
0	2.028	1.59	0.49	0.80	1.15	2.81	0.29	6.57	6.44	9.64	7.89	0.169
0.01	2.032	1.76	0.49	0.88	1.13	2.66	0.28	5.83	6.01	8.90	7.10	0.145
0.025	2.315	1.98	0.50	0.99	1.21	2.47	0.27	4.67	5.97	7.81	6.12	0.163
0.05	2.306	2.20	0.50	1.10	1.15	2.29	0.25	3.93	5.25	7.10	5.24	0.200
0.075	2.707	2.21	0.51	1.11	1.33	2.28	0.27	3.45	6.05	7.09	5.21	0.202
0.1	2.912	2.23	0.51	1.12	1.40	2.26	0.28	3.16	6.35	7.06	5.13	0.205
0.15	3.053	2.44	0.51	1.22	1.33	2.09	0.26	2.58	5.57	7.35	4.36	0.223
0.2	3.233	2.29	0.52	1.14	1.49	2.22	0.29	2.70	6.60	7.04	4.92	0.213
0.25	3.318	2.36	0.51	1.18	1.46	2.16	0.29	2.52	6.31	7.11	4.66	0.220
0.3	3.724	2.44	0.51	1.22	1.61	2.09	0.31	1.75	6.74	7.36	4.35	0.223
0.35	3.353	2.44	0.49	1.22	1.53	2.09	0.30	2.02	6.39	7.35	4.36	0.223
0.4	2.959	2.50	0.50	1.25	1.27	2.04	0.25	2.52	5.18	7.67	4.14	0.220

Table 5.2. Electrical characteristics of the CoS and $Co_{1-x}Zn_XS$ ($0 \leq x \leq 0.4$) thin films.

Composition (x)	Activation Energy eV		Thermal Eg, eV	E_{Ac} eV	Barrier Potential (Φ_B) eV	Carrier concentration, n x 10^{19} cm^{-3}	Carrier mobility μ x 10^{-4} $cm^2/V.s$
	HT	LT					
0	0.869	0.065	1.74	0.130	0.452	6.092	1.25
0.01	0.917	0.092	1.84	0.184	0.479	6.090	1.19
0.025	0.933	0.096	1.87	0.192	0.510	6.089	1.00
0.05	0.969	0.097	1.94	0.194	0.525	6.088	0.88
0.075	0.977	0.102	1.95	0.204	0.530	6.088	0.78
0.1	1.004	0.111	2.01	0.222	0.538	6.087	0.65
0.15	1.017	0.122	2.03	0.244	0.546	6.087	0.63
0.2	1.018	0.127	2.04	0.254	0.543	6.087	0.60
0.25	1.022	0.137	2.04	0.274	0.537	6.087	0.70
0.30	1.023	0.155	2.05	0.310	0.529	6.087	0.72
0.35	1.024	0.161	2.05	0.322	0.526	6.087	0.41
0.40	1.026	0.155	2.05	0.310	0.520	6.088	0.33

References

[1] K.L. Chopra, Thin Film Technology and Applications, (Eds.), K.L. Chopra, L.K. Malhotra, T.M.H. Publishing Co., India 1 (1984).

[2] G. Hodes, Phys Chem Chem Phys 9 (2007) 2181.

[3] E. Shanthi, A. Banerjee, V. Dutta, K.L. Chopra, J Appl Phys 53 (1982) 1615.

[4] S. Chandra, Photoelectrochemical Solar Cells, (Eds.) D.S. Campbell, Golden and Breach Science Publication, New York, USA, (1985).

[5] L.P. Deshmukh, D.S. Sutrave, Mater Chem Phys 55 (1998) 30.

(a) M.D. Uplane, S.H. Pawar, Solar Cells 10 (1983) 177.

[6] Y. D. Tembhurkar, J.P. Hirde, Thin Solid Films, 215 (1992) 65.

[7] L.P. Deshmukh, S.G. Holikatti, B.M. More, Mat Chem Phys 39 (1995) 278.

[8] L.P. Deshmukh, K.V. Zipre, A.B. Palwe, Sol Ener Mat & Sol Cells 28 (1992) 249.

[9] A.N. Chattarki, N.N. Maldar, L.P. Deshmukh, J Alloys Compd 597 (2014) 223.

[10] A.N. Chattarki, S.S. Kamble, L.P. Deshmukh, Mater Lett 67 (2012) 39.

[11] S.T. Mane, P.C. Pingale, R.V. Suryawanshi, V.S. Karande, L.P. Deshmukh, M. Sharon, Electrochim Acta 114 (2013) 494.

[12] S.T. Mane, P.C. Pingale, S.A. Lendave, V.S. Karande, L.P. Deshmukh, M. Sharon, Electrochim Acta 102 (2013) 113.

[13] S.T. Mane, S.S. Kamble, L.P. Deshmukh, Mater Lett 65 (2011) 2639.

[14] S.S. Kamble, A. Sikora, S.T. Pawar, R.C. Kambale, N.N. Maldar, L.P. Deshmukh, J Alloys Compd 631 (2015) 303.

[15] S.S. Kamble, Andrzej Sikora, S.T. Pawar, N.N. Maldar, L.P. Deshmukh, J Alloys Compd 623 (2015) 466.

[16] S.S. Kamble, A. Sikora, S.T. Pawar, G.T. Chavan, N.N. Maldar, L.P. Deshmukh, Some Investigations on $Zn_xCo_{1-x}S$ DMS Thin Films: Chemical Synthesis and Characteristic Properties, 2nd International Symposium on Physics and Technology of Sensors (ISPTS-2), 08-10 March 2015, Pune, India.

[17] D. Bhattacharya, S. Chaudhuri, A.K. Pal, Vacuum 43 (1992) 313.

[18] J.Y.W. Seto, J Appl Phys 46 (1975) 5247.

[19] J.W. Orton, M.J. Powell, Rep Progr Phys 43 (1980) 1263.

[20] N. F. Mott, Phil Mag 19 (1969) 835.

[21] L.I. Soliman, Ind. J Pure & Appl Phys 32 (1994) 166.

[22] J. Poortmans, V. Arkhipov (Eds.), Thin Film Solar Cells Fabrication, Characterization and Applications, Wiley Series in Materials for Electronic and Optoelectronic Applications, John Wiley & Sons Ltd, (2013).

[23] P. Sharma, S. Kumar, V. Sharma, Science of Advanced Materials 5 (2013) 713.

[24] J. Kossut, J.A. Gaj, (Eds.), Introduction to the Physics of Diluted Magnetic Semiconductors, Springer Series in Materials Science, 144 (2010).

[25] S. Kumar, P. Sharma, V. Sharma, J Nanopart Res 15 (2013) 1662.

[26] J. Luengo, N.V. Joshi, Mater Lett 26 (1996) 47-50.

[27] P. Sharma, S.C. Katyal, J Phys D: Appl Phys 40 (2007) 2115.

[28] A.R. Forouhi, I. Bloomer, Phys Rev B38 (1988) 1865.

[29] N.A. Bakr, A.M. Funde, V.S. Waman, M.M. Kamble, R.R. Hawaldar, D.P. Amalnerkar, S.W. Gosavi, S.R. Jadkar, Pramana - Journal of Physics, 76 (2011) 519.

[30] A. Goswami (Eds.), Thin film fundamentals, New Age International, New Delhi, India (2005).

[31] K.L. Chopra, S.R. Das, Thin Film Solar Cells, (Eds.) K.L. Chopra, S.R. Das, Plemun Press, New York, USA (1983).

[32] S. Mohan (Eds.), Advanced Course on Thin Film Processing, Instrumentation and Services Unit, I.I.Sc., Bangalore, India (1994).

[33] N.F. Mott, E.A. Davis (Eds.), Electronic processes in non-crystalline materials, Oxford: Mott and Davis Clarendon Press (1971).

[34] Oumous, H. Hadiri, Thin Solid Films 386 (2001) 87.

[35] S.A. Lendavc, V.S. Karande, L.P. Deshmukh, J Metallurgy & Mat Sci 52 (2010) 363.

[36] S.A. Lendave, Ph.D. Thesis, Solapur University, Solapur (M.S.) India (2011).

[37] M.M.A. Sekkina, A. Tawfik, M.I.A. El-Ali, Thermochimica Acta 86 (1985) 59.

[38] L.P. Deshmukh, Ph.D. Thesis, Shivaji University, Kolhapur, M. S. India (1985).

[39] M.M.H. Farooqi, R.K. Srivastava, Materials Science in Semiconductor Processing 20 (2014) 61.

[40] R. Kripal, A.K. Gupta, S.K. Mishra, R.K. Srivastava, A.C. Pandey, S.G. Prakash, Spectrochim Acta: Part A 76 (2010) 523.

[41] K. Sheo, R. Mishra, K. Srivastava, S.G. Prakash, J Alloys Compd 1 (2012) 539.

[42] R. Kaiwaga, T. Uesugi, T. Yoshida, S. Merdes, R. Klenk, Thin Solid Films, 517 (2009) 2184.

[43] N. Badera, B. Godbole, S.Srivastava, P. Vishwakarma, L. Sharath, D. Jain, V. Sathe, V. Ganesan, Sol Ener Mat & Sol Cells 92 (2008) 1646.